Acta Pharmaceutica Sinica B 2024;14(7):2942–2958

Chinese Pharmaceutical Association
Institute of Materia Medica, Chinese Academy of Medical Sciences

Acta Pharmaceutica Sinica B

www.elsevier.com/locate/apsb
www.sciencedirect.com

ORIGINAL ARTICLE

LncRNA ZFPM2-AS1 promotes phyllodes tumor progression by binding to CDC42 and inhibiting STAT1 activation

Shishi He[a,b,†], Guowei Huang[c,†], Rong Lei[a,b,†], Rurong Jia[d,b], Zhanghai He[e], Jiewen Chen[f], Hongyan Huang[g], Zixian Huang[a,h], Ailifeire Yilihamu[a,b], Xun Li[a,b], Zilin Zhuang[a,b], Mengjia Han[a,b], Xueman Chen[a,b,*], Di Huang[a,b,*], Yan Nie[a,b,*]

[a]*Guangdong Provincial Key Laboratory of Malignant Tumor Epigenetics and Gene Regulation, Guangdong-Hong Kong Joint Laboratory for RNA Medicine, Medical Research Center, Sun Yat-sen Memorial Hospital, Sun Yat-sen University, Guangzhou 510120, China*
[b]*Breast Tumor Center, Sun Yat-sen Memorial Hospital, Sun Yat-sen University, Guangzhou 510120, China*
[c]*Department of Pathology, Shantou University Medical College, Shantou 515041, China*
[d]*School of Basic Medical Science, Southern Medical University, Guangzhou 510515, China*
[e]*Department of Pathology, Sun Yat-sen Memorial Hospital, Sun Yat-sen University, Guangzhou 510120, China*
[f]*Department of Breast Medicine, Affiliated Foshan Maternity and Child Healthcare Hospital, Southern Medical University, Foshan 528000, China*
[g]*Department of Breast Surgery, Zhujiang Hospital, Southern Medical University, Guangzhou 510282, China*
[h]*Department of Oral and Maxillofacial Surgery, Sun Yat-sen Memorial Hospital, Sun Yat-sen University, Guangzhou 510120, China*

Received 26 February 2024; received in revised form 14 April 2024; accepted 15 April 2024

KEY WORDS

LncRNA;
Phyllodes tumor;
ZFPM2-AS1;
Cell division cycle 42;
Activated cdc42 kinase 1;

Abstract Breast phyllodes tumor (PT) is a rare fibroepithelial neoplasm with potential malignant behavior. Long non-coding RNAs (lncRNAs) play multifaceted roles in various cancers, but their involvement in breast PT remains largely unexplored. In this study, microarray was leveraged for the first time to investigate the role of lncRNA in PT. We identified lncRNA ZFPM2-AS1 was significantly upregulated in malignant PT, and its overexpression endowed PT with high tumor grade and adverse prognosis. Furthermore, we elucidated that ZFPM2-AS1 promotes the proliferation, migration, and invasion of malignant

*Corresponding authors.
E-mail addresses: chenxm223@mail.sysu.edu.cn (Xueman Chen), huangd63@mail.sysu.edu.cn (Di Huang), nieyan7@mail.sysu.edu.cn (Yan Nie).
[†]These authors made equal contributions to this work.
Peer review under the responsibility of Chinese Pharmaceutical Association and Institute of Materia Medica, Chinese Academy of Medical Sciences.

https://doi.org/10.1016/j.apsb.2024.04.023

Signal transducer and activator of transcription 1;
TNF receptor superfamily member 19;
Nano particles

PT *in vitro*. Targeting ZFPM2-AS1 through nanomaterial-mediated siRNA delivery in patient-derived xenograft (PDX) model could effectively inhibit tumor progression *in vivo*. Mechanistically, our findings showed that ZFPM2-AS1 is competitively bound to CDC42, inhibiting ACK1 and STAT1 activation, thereby launching the transcription of TNFRSF19. In conclusion, our study provides evidence that ZFPM2-AS1 plays a pivotal role in the pathogenesis of breast PT, and suggests that ZFPM2-AS1 could serve as a prognostic indicator for patients with PT as well as a promising novel therapeutic target.

1. Introduction

Breast phyllodes tumor (PT) is a rare fibroepithelial tumor, accounting for only 0.3%−1% of all primary breast tumors[1]. The World Health Organization classifies PT into three categories based on clinicopathological features: benign, borderline, and malignant[2]. Patients with PT are at high risk of recurrence, with rates ranging from 3.4% to 20.8% for benign PT, 14.1%−41.7% for borderline PT, and 42.3%−65% for malignant PT[3,4,5]. In addition, recurrent PT may progress to a more malignant phenotype[6]. However, PT is not sensitive to conventional radiotherapy or chemotherapy[7,8], and there are no effective therapeutic targets available for treatment. Therefore, exploring the mechanism underpinning the malignant progression of PT is essential for effective cancer therapy.

LncRNAs, a large class of non-coding RNAs with more than 200 bp in length, are characterized by spatial and temporal-specific expression patterns, playing crucial roles in the regulation of gene expression[9,10]. In recent years, some lncRNAs, such as MALAT1 and HOTAIR, which are highly expressed in a variety of tumors, have been found to be crucial for tumor proliferation, migration, invasion, clinical staging, and prognosis[11,12]. However, the role of lncRNA in PT has not been delineated.

In this study, we aimed to excavate lncRNAs associated with PT malignant progression and patient prognosis. Our results showed that ZFPM2-AS1 expression increased with the malignant degree of PT, and patients with higher ZFPM2-AS1 expression were more prone to tumor progression and shorter survival time. In mechanism, our data uncovers that ZFPM2-AS1 binds with CDC42, leading to inhibition of the phosphorylation and the downstream signaling of ACK1 and STAT1, and thereby promotes tumor progression. Collectively, these findings disclose that ZFPM2-AS1 could serve as prognosis prediction marker and therapeutic target for PT.

2. Materials and methods

2.1. Patients and tissue samples

Breast tumor samples were obtained from the Breast Tumor Center of Sun Yat-sen Memorial Hospital, Sun Yat-sen University (Guangzhou, China). A total of 193 surgically resected PTs and 4 fibroadenomas were employed between 2011 and 2022. Patients were followed up for a duration of 1−125 months, with a median follow-up of 44 months. Pathological diagnoses were independently corroborated by two qualified pathologists. All human samples were collected with the informed consent of the donors. And our study was approved by Sun Yat-sen Memorial Hospital, Sun Yat-sen University Ethics Committee, and the approval number is SYSEC-KY-KS-2021-377.

2.2. RNA preparation and microarray analysis

Surgically resected tumor specimens (including 4 FAs, 6 benign PTs, and 6 malignant PTs) were immediately immersed in RNA preservation solution and frozen in liquid nitrogen to preserve RNA integrity. Frozen samples were then stored at −80 °C until further analysis. Total RNA was extracted from the PT samples using Trizol reagent, a widely used isolation method. Agilent Human lncRNA and mRNA Microarray was used for global profiling of human lncRNA and mRNA. The microarray analysis was conducted by Geneway Decoding Bio-Tech company (Guangzhou, China).

2.3. Quantitative real-time PCR (qRT-PCR)

Reverse transcription was performed with HiScript ®II Q RT SuperMix (Vazyme, Nanjing, China). qRT-PCR assays were performed with ChamQ SYBR® qPCR Master Mix (Vazyme). The primer sequences were displayed in Supporting Information Table S1.

2.4. Rapid amplification of cDNA ends (RACE)

To facilitate the amplification, a polyA tail was added to the 3′ end of the RNA using the Poly(A) enzyme. Then, we employed the HiScript TS 5′/3′ RACE Kit (Vazyme) to rapidly amplify the cDNA ends of the RNA samples. The resulting DNA products were then purified using a gel recovery/DNA purification kit (Vazyme) as per the manufacturer's instructions. The purified DNA fragments were subsequently inserted into plasmids and introduced into Fast-T1 competent cells (Vazyme). The competent cells were then inoculated into LB solid medium, and monoclonal colonies were selected for sequencing by BGI company.

The sequences of Gene Specific Primers (GSP) were as follows:

5′ GSP: TCAGCCTGTATGTCTTCTCCAAGTTCCA.
3′ GSP: GGAACTTGGAGAAGACATACAGGC.

2.5. In situ hybridization (ISH)

Paraffin sections of 193 PTs were obtained from the Breast Tumor Center of Sun Yat-sen Memorial Hospital, Sun Yat-sen University. ISH experiments were performed following the instructions of the Enhanced Sensitive ISH Detection Kit II (Boster, Wuhan, China). Digoxin-labeled lncRNA probe (QIAGEN, Dusseldorf, Germany)

was used at a concentration of 50 nmol/L and the hybridization temperature was 37 °C.

The ISH score was determined through combining the percentage of positively stained tumor cells and the staining intensity of positively stained tumor cells. Combined with the survival prognosis information, the optimal threshold of ZFPM2-AS1 expression was analyzed by X-tile software.

The sequence of the ISH probe: TGCGATTAGCTTCTAT GCCTT.

2.6. Nuclear plasma separation experiment

The nuclear plasma separation experiment was conducted following the instructions provided in the PARIS Kit (Invitrogen, CA, USA). The isolated nuclear components were treated with Trizol for RNA extraction, while the cytoplasmic components were treated with Trizol LS (Invitrogen) for RNA extraction. MALAT1 and β-actin were used as reference genes for the nucleus and cytoplasm, respectively.

2.7. Fluorescence in situ hybridization (FISH)

Cells were cultured in a confocal dish, and Cy3-labeled FISH probes (Ribo, Guangzhou, China) were used following the instructions provided in the Fluorescence In Situ Hybridization Kit (Ribo). U6 was utilized as the positive control for nuclear staining, while 18S was used as the positive control for cytoplasmic staining.

2.8. Cell cultures and treatment

The PT primary cells were isolated following the previously described protocol[13]. Human benign PT cell lines, SYSH-BPT-01, and malignant PT cell lines, SYSH-MPT-01 and SYSH-MPT-02, were established by immortalization, STR identification showed each PT cell line was homologous to parental primary cells[14]. The cell lines were cultured in DMEM/F12 medium supplemented with 15% fetal bovine serum, 20 ng/mL epidermal growth factor, 0.5 mg/mL hydrocortisone, and 10 μg/mL insulin. All cells were tested for mycoplasma, the results were negative.

2.9. Cell transfection

Lipofectamine 3000 (Invitrogen) was employed for the transfection of siRNA or plasmid. The control siRNA sequence was as follows:

NC: 5′- UUCUCCGAACGUGUCACGU-3′.

The ZFPM2-AS1 siRNA sequences were as follows:

ZFPM2-AS1#1: 5′-GCAGAGAAGAUGAGAUCAU-3′

ZFPM2-AS1#2: 5′-GGGAGAGUAUGGAGUGAAA-3′

The CDC42 siRNA sequences were as follows:

CDC42#1: 5′-CCCUCUACUAUUGAGAAACUU-3′

CDC42#2: 5′-CGGAAUAUGUACCGACUGUUU-3′

The ACK1 siRNA sequence was as follows:

5′-GGUGUUCAGUGGAAAGCGACU-3′

The STAT1 siRNA sequence was as follows:

5′- CUGGAUAUAUCAAGACUGA -3′

ZFPM2-AS1 and its antisense, truncated sequences in pcDNA3.1 plasmid were Synthesized by IGE Biotechnology company, Guangzhou, China.

The promoter sequence of TNFRSF19 in pGL3-basic plasmid was Synthesized by Generay Biotech company, Shanghai, China.

After the previous screening, we selected ZFPM2-AS1#1 with high transfection efficiency. The recombinant lentiviral vector and packaging plasmid were transfected into 293T cells to obtain virus suspension. PT cells were infected by virus suspension. Stable PT cell lines with stably expressed short hairpin RNA ZFPM2-AS1 (sh-ZFPM2-AS1) were obtained by G418 (APExBio, Houston, USA) screening, and a shRNA negative control group (sh-control) was also prepared.

2.10. Proliferation assay and colony formation assays

For the cell proliferation assays, a total of 2000 cells were seeded into 96-well plates. CCK8 (APExBio) was added and the plates were incubated at 37 °C for 2 h, followed by the detection of optical density (OD) values at 450 nm.

For the colony formation assays, 100 cells were seeded into 6-well plates. After 10 days of culture, the cells were fixed with 4% paraformaldehyde, stained with crystal violet, and the colonies were counted.

2.11. Cell migration and invasion assays

In the migration assays, firstly, we treated the cells with mitomycin (1 μg/mL, Selleck, Houston, USA) for 1 h to avoid the effect caused by cell proliferation. Then, 2×10^4 cells were seeded into the upper chambers of transwell inserts (Corning, NY, USA) with serum-free culture medium, while the lower chambers were filled with complete medium. After 24 h of culture, the upper chambers were fixed with 4% paraformaldehyde and stained with crystal violet. For the invasion assay, the upper chambers were pre-coated with 20% Matrigel (BD, NY, USA), and the subsequent steps were performed as described above. Migrated and invasive cells were counted in 5 randomly selected fields at 200 × magnification.

2.12. RNA pull-down

In vitro transcription was conducted according to the instructions provided in the MEGAscript T7 transcription kit (Invitrogen). Proteins were extracted using IP Lysis Buffer (Invitrogen). The *in vitro* transcribed RNA was then incubated with proteins at room temperature for 2 h, and the M-280 magnetic beads (Invitrogen) were used to enrich biotin-labeled RNA and bound proteins. The enriched proteins were analyzed by mass spectrum.

The enriched proteins were separated by electrophoresis in MOPS electrophoresis buffer. Subsequently, the gel was transferred to a clean petri dish and stained with Coomassie brilliant blue staining solution for 1 h, followed by decolorization with a decolorizing solution containing methanol and glacial acetic acid.

2.13. RNA immunoprecipitation (RIP)

The proteins were extracted using IP Lysis Buffer (Invitrogen) supplemented with protease, phosphatase, and RNase inhibitors. It was then mixed with the CDC42 antibody (1:20, Abcam, Cambridge, UK) and incubated at room temperature for 2 h. Antibody and its binding proteins and RNA were enriched with protein A/G magnetic beads (Invitrogen). Subsequently, the proteins were removed by protease K treatment, and RNA was extracted by adding Trizol LS. Normal Rabbit IgG (Cell signaling, Boston, USA) was used as a control.

2.14. Western blot

Proteins were extracted from cells and tissues using RIPA buffer supplemented with phosphatase inhibitor and protease inhibitor. WB was performed using SDS-poly acrylamide gel electrophoresis (SDS-PAGE), PVDF membrane according to standard procedures. The primary antibodies used in this experiment included phospho-ACK1 (1:500, Abcam), total ACK1 (1 μg/mL, Abcam), phospho-STAT1 (1:1000, Cell signaling), total STAT1 (1:1000, Cell signaling, Boston, USA), CDC42 (1:1000, Abcam), TNFRSF19 (1:1000, Abcam), and GAPDH (1:5000, Proteintech, Chicago, USA).

2.15. RNA sequencing

After ZFPM2-AS1 knockdown, RNA was extracted from malignant PT cell lines and primary cells, and RNA-sequencing was performed by Anoroad company (Beijing, China).

2.16. Dual luciferase reporter assays

The PT cells were subjected to different treatments, including treatment with IFNγ (PeproTech, NJ, USA) or transfection with ZFPM2-AS1 or STAT1 siRNA. Then, TNFRSF19 in pGL3-basic plasmid and phRL-TK plasmid was transfected into PT cell lines, as per standard transfection protocols. Luciferase activities were measured using the Dual-Luciferase Reporter Assay Kit (Vazyme) in accordance with the manufacturer's instructions.

2.17. Preparation and characterizations of nanoparticles (NPs)

The NPs-NC siRNA and NPs-ZFPM2-AS1 siRNA were prepared according to the previous report[15]. The G0 C14 solution (5 mg/mL in *N*,*N*-dimethylformamide) and siRNA solution (0.1 nmol/μL in sterile water) were mixed, left for 3 min, and then added to methoxyl-poly (ethylene glycol)-*b*-poly (2-(diisopropylamino) ethyl methacrylate) (Meo-PEG-*b*-PDPA) solution (20 mg/mL in *N*,*N*-dimethylformamide). The above mixture was added to deionized water and stirred continuously, followed by transferring to ultrafiltration tube (Millipore, Boston, USA) and centrifuged to remove organic solvents and free compounds. siRNAs loaded NPs were obtained after washing three times with deionized water. The size and zeta potential of NPs were determined by dynamic light scattering (Brookhaven Instruments Corporation).

2.18. Animal experiments

All animal experiments were conducted in accordance with the legal mandates and national guidelines for the care and maintenance of laboratory animals and were approved by the Animal Ethical and Welfare Committee, Sun Yat-sen Memorial Hospital, Sun Yat-sen University (AP20220134). Mice were housed in a specific pathogen-free animal house at 28 °C and 50% humidity.

The detailed procedure for establishing the patient-derived xenograft (PDX) model was described previously[13]. In brief, 6-week-old NOD-SCID female mice (gempharmatech Co., Ltd. Guangzhou, China) were anesthetized with isoflurane, and the malignant PT samples were minced into 1 mm^3-sized fragments and directly embedded into the mammary fat pads.

Once the PDX tumors reached a diameter of 1 mm, the mice were randomly divided into three groups ($n = 8$) and received daily intravenous injections of either PBS, NPs-NC siRNA, or NPs-ZFPM2-AS1 siRNA (1 nmol siRNA per mouse). After three consecutive injections, the size of the PDX tumors was measured every three days. The mice were euthanized 15 days after injection, and the tumors were removed for measurement and photography.

2.19. Pharmacokinetics study

Healthy 6-week-old female BALB/c mice (gempharmatech Co., Ltd.) were randomly assigned to two groups ($n = 3$), and each mouse was intravenously injected with either Cy5 labeled naked-siRNA or NPs-siRNA (1 nmol per mouse). Following the injection, 20 μL of orbital vein blood was withdrawn using a heparin-containing tube. The Cy5 intensity in the blood was measured using a microplate reader.

2.20. Biodistribution

PDX mice of PT were randomly assigned to two groups ($n = 3$) and were intravenously injected with either Cy5 labeled naked-siRNA or NPs-siRNA (1 nmol per mouse). After 24 h, the Cy5 intensity in tissue homogenates were measured using a microplate reader to quantify the accumulation of siRNA in PTs and organs.

2.21. Histology and hematology

Healthy 6-week-old female BALB/c mice (Gempharmatech Co., Ltd.) were randomly divided into three groups ($n = 3$) and were intravenously injected with either PBS, NPs-NC siRNA, or NPs-ZFPM2-AS1 siRNA (1 nmol per mouse). The main organs were collected after three consecutive injections. Organ tissue sections were stained with hematoxylin-eosin (H&E). Blood samples were collected for examination of AST, ALT, ALP, Urea, CREA, and ALB levels to assess the potential effects on liver and kidney function.

2.22. Lung metastasis assays

The healthy 6-week-old NOD-SCID female mice were divided into two groups (7 mice per group): sh-control and sh-ZFPM2-AS1. The corresponding cells (10^7 cells per mouse) were injected into the mice through the tail vein, and the lungs were removed 1 month later to observe the metastasis.

2.23. Statistical analysis

Statistical analysis was conducted using GraphPad Prism 6 software (GraphPad Software Inc., USA) and SPSS 16.0 statistical software package. The χ^2 test was used to analyze the relationship between ZFPM2-AS1 expression and clinicopathologic status of PTs. Kaplan−Meier curves and log-rank test were utilized to compare Disease-free survival (DFS) and overall survival (OS) among different patient groups. Cox regression analysis was employed to assess the hazard ratio of ZFPM2-AS1 expression and clinicopathological features on disease progression and patient survival.

The data were presented as mean ± standard deviation (SD) from three independent experiments performed in triplicate. Statistical differences were analyzed using the unpaired two-tailed Student's *t*-test. Statistical significance was defined as $^*P < 0.05$, $^{**}P < 0.01$, $^{***}P < 0.001$.

2.24. Data availability

All data needed to evaluate the conclusions in the paper are present in the paper and/or the Supporting Information. The mRNA and lncRNA Microarrays, RNA sequencing data have been deposited to the GEO database with the dataset identifiers GSE235267 and GSE235268, respectively.

3. Results

3.1. Highly-expressed ZFPM2-AS1 in malignant PT is significantly associated with poor prognosis

To identify lncRNA dictating progression of PT, mRNA and lncRNA Microarray analysis for 4 fibroadenomas, 6 benign PTs, and 6 malignant PTs was conducted. Based on the criteria of $|\mathrm{Log_2FC}| \geq 2$ and $P < 0.05$, we identified 100 lncRNAs that were significantly differentially expressed in malignant PTs compared to fibroadenomas and benign PTs, with 38 upregulated lncRNAs and 62 downregulated lncRNAs (Fig. 1A and B, Supporting Information Fig. S1A, Table S2). The top five upregulated and downregulated lncRNAs were subsequently validated by qRT-PCR using RNA extracted from PT cell lines (SYSH-BPT-01, SYSH-MPT-01, and SYSH-MPT-02) and freshly frozen PT tissues ($n = 115$). The results revealed that the expression levels of LINC00189 and ZFPM2-AS1 were significantly increased with tumor grade, and ZFPM2-AS1 showed a more pronounced upregulation in contrast to LINC00189 (Fig. 1C, Fig. S1B). Furthermore, the data from The Cancer Genome Atlas (TCGA) database revealed that highly-expressed ZFPM2-AS1 was significantly associated with poor prognosis in low-grade glioma (LGG), cervical squamous cell carcinoma (CESC), stomach adenocarcinoma (STAD), liver hepatocellular carcinoma (LIHC), sarcoma (SARC), and uterine corpus endometrial carcinoma (UCEC) (Fig. 1D), indicating that ZFPM2-AS1 may play a critical role in the malignant phenotype of tumors.

To further delineate the full length of ZFPM2-AS1 in PT, we conducted rapid amplification of cDNA ends (RACE) assays with PT cells. A novel transcript of ZFPM2-AS1 with full-length 1001 nt and without a polyA tail was observed (Fig. S1C), which differs from the two transcripts NR_125796 and NR_125797 annotated in the NCBI database (Fig. 1E). The Coding Potential Calculator 2 tool was employed to assess the encoding capacity of this novel transcript sequence, which revealed that the novel identified transcript had a weak encoding ability, confirming its nature as a non-coding RNA (Fig. S1D). Furthermore, qRT-PCR analysis using transcriptional-specific primers indicated that ZFPM2-AS1 was exclusively expressed as the novel identified transcript in PT (Fig. S1E). Moreover, we performed *in situ* hybridization (ISH) in 62 benign, 69 borderline, and 62 malignant PTs. Consistent with previous findings, the expression of ZFPM2-AS1 significantly increased with increasing tumor malignancy (Fig. 1F). We further categorized the PT patients into high or low ZFPM2-AS1 expression group based on the ISH scores. The survival curve showed that patients with highly-expressed ZFPM2-AS1 had significantly worse outcomes and shorter survival time (Fig. 1G). Correlation analysis showed that expression of ZFPM2-AS1 was significantly correlated with the pathologic indicators such as tumor size ($P < 0.001$), grade ($P < 0.001$), border ($P < 0.001$), mitotic ($P < 0.001$), atypia ($P < 0.001$) and stromal overgrowth ($P = 0.001$) of PTs and also obviously associated with local recurrence ($P < 0.001$), distant metastasis ($P < 0.001$) and death ($P < 0.001$) of PT patients (Table 1). Cox regression analysis revealed that highly-expressed ZFPM2-AS1 and marked atypia were independent prognostic indicators for local recurrence and metastasis in PT patients (Table 2), while highly-expressed ZFPM2-AS1, large tumor size, and high mitotic activity were independent prognostic indicators for death in PT patients (Table 3). Overall, these results demonstrated that ZFPM2-AS1 expression was significantly increased in malignant PT and associated with poor prognosis in PT patients, suggesting that ZFPM2-AS1 may be a critical contributor to the malignant phenotype of tumors.

3.2. ZFPM2-AS1 is mainly distributed in cytoplasm and promotes proliferation, migration, and invasion of PT cells

To interrogate the role of ZFPM2-AS1, we first examined its cellular localization. Nuclear plasma separation experiments revealed that ZFPM2-AS1 was present in both the nucleus and cytoplasm, with a higher abundance in the latter (Fig. 2A). Fluorescence *in situ* hybridization (FISH) assays also confirmed that ZFPM2-AS1 was primarily localized in the cytoplasm in both PT cell lines and primary PT cells (Fig. 2B, Supporting Information Fig. S2A). To further investigate the fundamental biological function of ZFPM2-AS1, we performed cell proliferation assays after knockdown or overexpression of ZFPM2-AS1 in malignant and benign PT cells (Fig. 2C, Fig. S2B). The results unveiled that ZFPM2-AS1 knockdown distinctly mitigated the proliferation of malignant PT cell lines, while its overexpression ameliorated the proliferation of benign PT cells (Fig. 2D, Fig. S2C). Clonal formation assays also indicated that ZFPM2-AS1 knockdown distinctly brought down the clonal formation ability of malignant PT cells (Fig. 2E, Fig. S2D), as anticipated, its overexpression enhanced that of benign PT cells (Fig. 2F). Additionally, we found that the cells with depletion of ZFPM2-AS1 formed smaller clones than the control group, while the cells that overexpressed ZFPM2-AS1 formed larger clones than the control group. We speculate that the difference in the size of clones is caused by the greater proliferation and growth ability of the cells with overexpressed ZFPM2-AS1 in comparison with the control group, so the cells with overexpressed ZFPM2-AS1 are more likely to form larger clones than the corresponding control group. Furthermore, Transwell experiments corroborated that siRNA loss-of-function for ZFPM2-AS1 significantly suppressed the migration and invasion of malignant PT cells (Fig. 2G, Fig. S2E), whereas its overexpression greatly promoted the migration and invasion of benign PT cells (Fig. 2H). These results give a hint that ZFPM2-AS1 endows PT cells with malignant biological behavior and promotes their aggressiveness.

3.3. ZFPM2-AS1 competitively binds to CDC42 to disrupt the interaction of ACK1 with CDC42

To gain further insight into the mechanism of ZFPM2-AS1 promoting the malignant progression of PT, we initially knocked down ZFPM2-AS1 in PT cells and performed transcriptome sequencing. Pathway enrichment analysis using Gene Set Enrichment Analysis (GSEA) revealed significant up-regulation of interferon signaling pathways and RHO GTPases activating ROCKs pathway after ZFPM2-AS1 knockdown (Fig. 3A, Supporting Information Fig. S3A and S3B). However, despite that

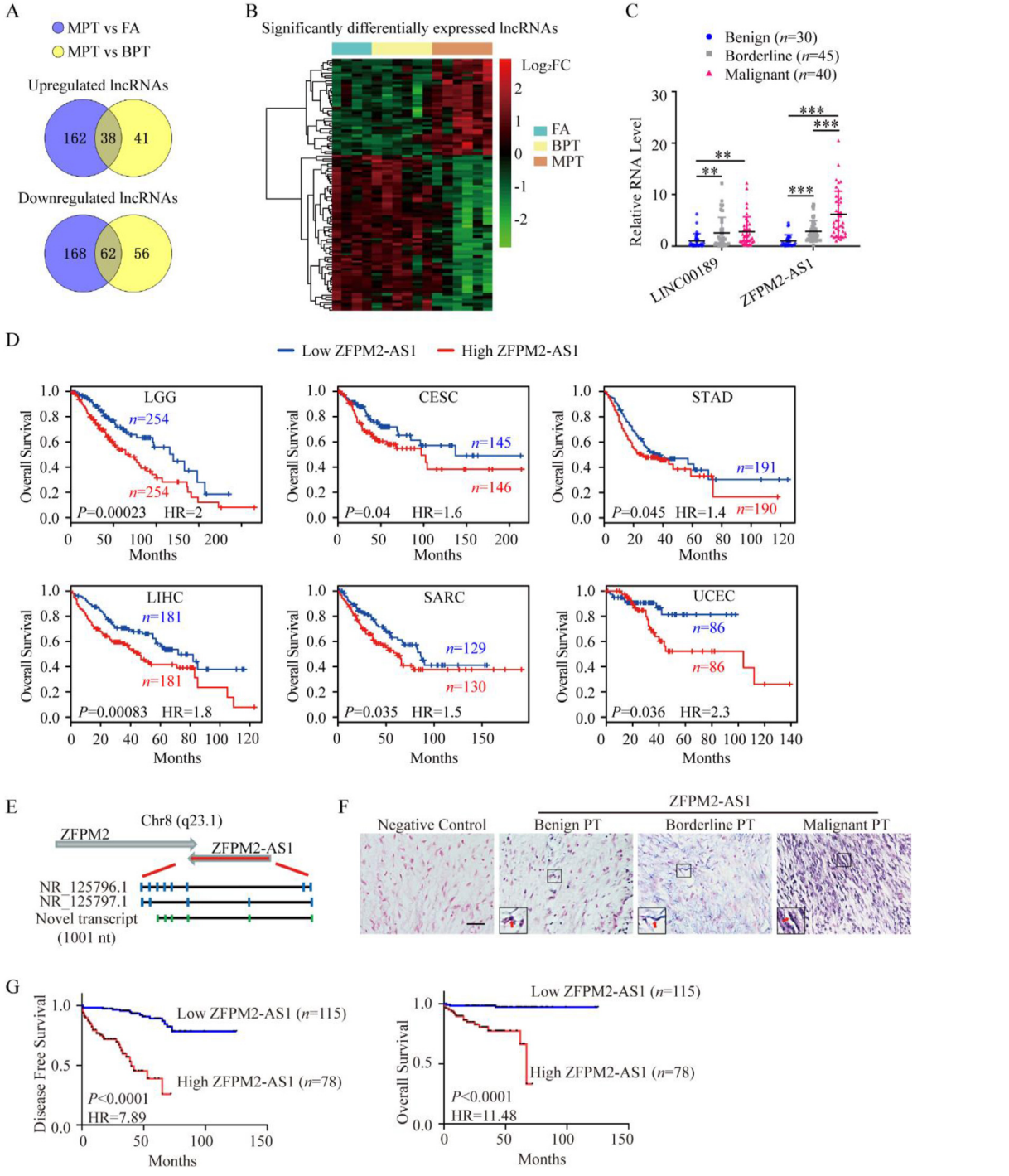

Figure 1 Highly-expressed ZFPM2-AS1 in malignant PT is significantly associated with poor prognosis. (A) The intersection of lncRNAs that were significantly differentially expressed in MPT compared with FA (blue) or BPT (yellow) in lncRNA chips, 38 up-regulated lncRNAs and 62 down-regulated lncRNAs were obtained. (FA: fibroadenoma, BPT: benign phyllodes tumor, MPT: malignant phyllodes tumor). (B) Heatmaps for 100 significantly differentially-expressed lncRNAs in MPT. (C) The expression levels of LINC00189 and ZFPM2-AS1 were detected by using qRT-PCR in breast PT freshly frozen tissue, both LINC00189 and ZFPM2-AS1 were significantly higher expressed in MPT than BPT. Data was shown as mean ± SD. $*P < 0.05$, $**P < 0.01$, and $***P < 0.001$. (D) Survival analysis of the TCGA database showed that high expression of ZFPM2-AS1 was associated with poor prognosis of low-grade glioma (LGG), cervical squamous cell carcinoma (CESC), stomach adenocarcinoma (STAD), liver hepatocellular carcinoma (LIHC), sarcoma (SARC), and uterine corpus endometrial carcinoma (UCEC). (E) Schematic diagram indicating the genomic location of the novel transcript of ZFPM2-AS1. (F) Representative images for ISH staining of ZFPM2-AS1 in benign PTs ($n = 62$), borderline PTs ($n = 69$), and malignant PTs ($n = 62$). A blue-purple color represents ZFPM2-AS1 staining, increasing with the PT grade. Scale bar: 50 μm, red arrows indicate ZFPM2-AS1 expression in cells. (G) Kaplan−Meier survival curves showed that patients with high expression of ZFPM2-AS1 were more prone to tumor progression and death.

Table 1 Correlations between ZFPM2-AS1 expression and clinicopathologic characteristics of breast phyllodes tumors.

Character	ZFPM2-AS1		Total 193 cases	*P*
	SI < 4 (115 cases)	SI ≥ 4 (78 cases)		
Age (year)[a]	42.0 (36.0−47.0)	40.5 (34.8−49.0)	41.0 (35.5−47.5)	0.988
Size (cm)[a]	3.5 (2.0−5.5)	5.0 (3.0−8.6)	4.0 (2.5−6.3)	< 0.001
Grade				< 0.001
Benign	45	17	62	
Borderline	49	20	69	
Malignant	21	41	62	
Border				< 0.001
Well defined	60	16	76	
Permeative	55	62	117	
Mitotic[a]	5.0 (1.0−9.0)	11.5 (4.0−15.0)	5.0 (1.0−12.0)	< 0.001
Atypia				< 0.001
Mild	42	17	59	
Moderate	61	33	94	
Marked	12	28	40	
Stromal overgrowth				0.001
Absent	53	17	70	
Present	62	61	123	
Recurrence				< 0.001
No	102	50	152	
Yes	13	28	41	
Metastasis				< 0.001
No	112	63	175	
Yes	3	15	18	
Dead				< 0.001
No	112	62	174	
Yes	3	16	19	

[a]Data did not conform to a normal distribution and was displayed as Median (First Quartile-Third Quartile).

Table 2 Univariate and multivariate analysis of various disease progression prognostic parameters in patients with breast phyllodes tumors.

Parameter	Univariate analysis			Multivariate analysis		
	P	HR	95% CI	*P*	HR	95% CI
Age	0.010	1.036	1.008−1.065	0.095	1.024	0.996−1.054
Borderline	0.257	1.751	0.665−4.612	0.772	1.174	0.398−3.460
Malignant	< 0.001	6.202	2.556−15.050	0.108	2.845	0.796−10.173
ZFPM2-AS1	< 0.001	9.041	4.499−18.167	< 0.001	4.923	2.284−10.611
Size	< 0.001	1.133	1.070−1.199	0.251	1.043	0.970−1.122
Border	0.002	2.950	1.491−5.839	0.351	1.442	0.669−3.110
Mitotic	< 0.001	1.060	1.038−1.083	0.251	1.019	0.986−1.054
Moderate atypia	0.380	1.395	0.664−2.934	0.295	0.627	0.261−1.503
Marked atypia	0.013	2.851	1.246−6.524	0.016	0.252	0.082−0.771
Stromal overgrowth	0.016	2.265	1.165−4.405	0.142	1.758	0.828−3.734

Table 3 Univariate and multivariate analysis of various survival prognostic parameters in patients with breast phyllodes tumors.

Parameter	Univariate analysis			Multivariate analysis		
	P	HR	95% CI	*P*	HR	95% CI
Age	0.011	1.055	1.012−1.099	0.080	1.036	0.996−1.079
Borderline	0.926	/	/	−	−	−
Malignant	0.906	/	/	−	−	−
ZFPM2-AS1	< 0.001	14.251	3.896−52.133	0.026	5.317	1.227−23.040
Size	< 0.001	1.223	1.135−1.318	0.002	1.142	1.048−1.243
Border	0.019	4.381	1.270−15.114	0.692	1.324	0.330−5.313
Mitotic	< 0.001	1.081	1.051−1.113	0.017	1.051	1.009−1.095
Moderate atypia	0.136	4.855	0.607−38.829	0.595	1.805	0.205−15.939
Marked atypia	0.004	20.487	2.612−160.682	0.596	1.874	0.184−19.092
Stromal overgrowth	0.087	2.635	0.869−7.984	−	−	−

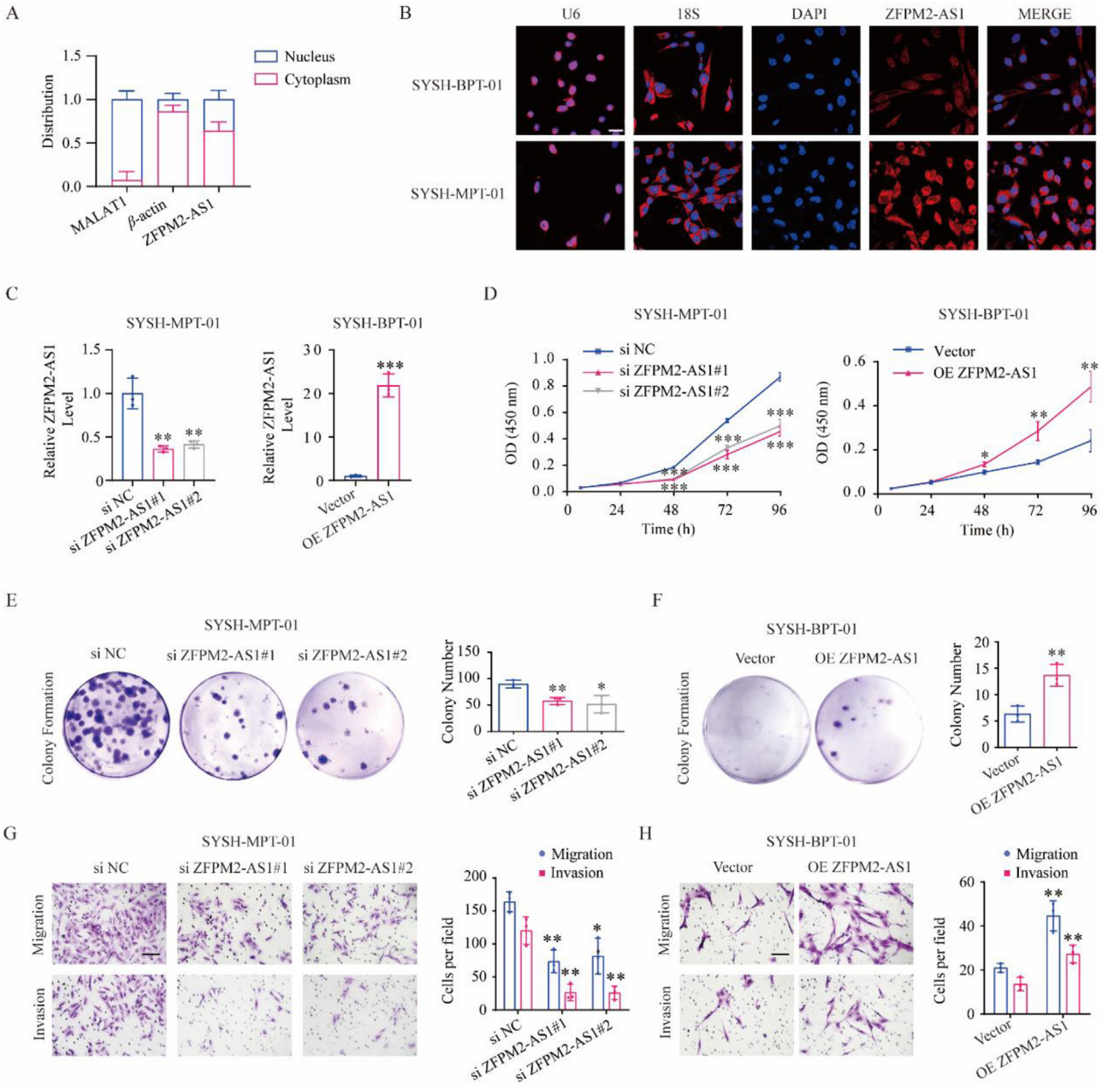

Figure 2 ZFPM2-AS1 is mainly distributed in cytoplasm and promotes proliferation, migration, and invasion of PT cells. (A) The distribution of ZFPM2-AS1 in PT cells was detected by qRT-PCR after nuclear plasma separation, ZFPM2-AS1 was distributed in both nucleus and cytoplasm, with more distribution in the cytoplasm (β-actin was used as cytoplasm reference and MALAT1 as nucleus reference). (B) FISH showed that ZFPM2-AS1 was primarily distributed in cytoplasm of PT cell lines (U6 was used as the nuclear positive control and 18S as the cytoplasmic positive control). Scale bar: 50 μm. (C) qRT-PCR showed that the knockdown efficiency of ZFPM2-AS1 by using siRNA in SYSH-MPT-01 was about 60%−70% (Left), and the efficiency of plasmid overexpression of ZFPM2-AS1 in SYSH-BPT-01 was about 20 times (Right). (D) Cell proliferation assays showed that the proliferation rate of SYSH-MPT-01 slowed down after ZFPM2-AS1 knockdown (Left), and the proliferation rate of SYSH-BPT-01 increased after overexpression of ZFPM2-AS1 (Right). (E, F) Colony formation assays showed that SYSH-MPT-01 formed less clones after ZFPM2-AS1 knockdown (E), while SYSH-BPT-01 formed more clones after ZFPM2-AS1 overexpression (F). (Left) Representative images of colony formation assays of PT cell lines. (Right) Bar chart showed the clones number of each group. (G, H) Transwell assays showed that the migration and invasion abilities of SYSH-MPT-01 decreased after ZFPM2-AS1 knockdown (G), while increased after ZFPM2-AS1 overexpression in SYSH-BPT-01 (H). (Left) Representative images of migration and invasion assays of PT cell lines. (Right) Bar chart showed the migrating cells and invading cells of each group. Data in (C)−(H) are shown as mean ± SD, $n = 3$. *$P < 0.05$, **$P < 0.01$, and ***$P < 0.001$.

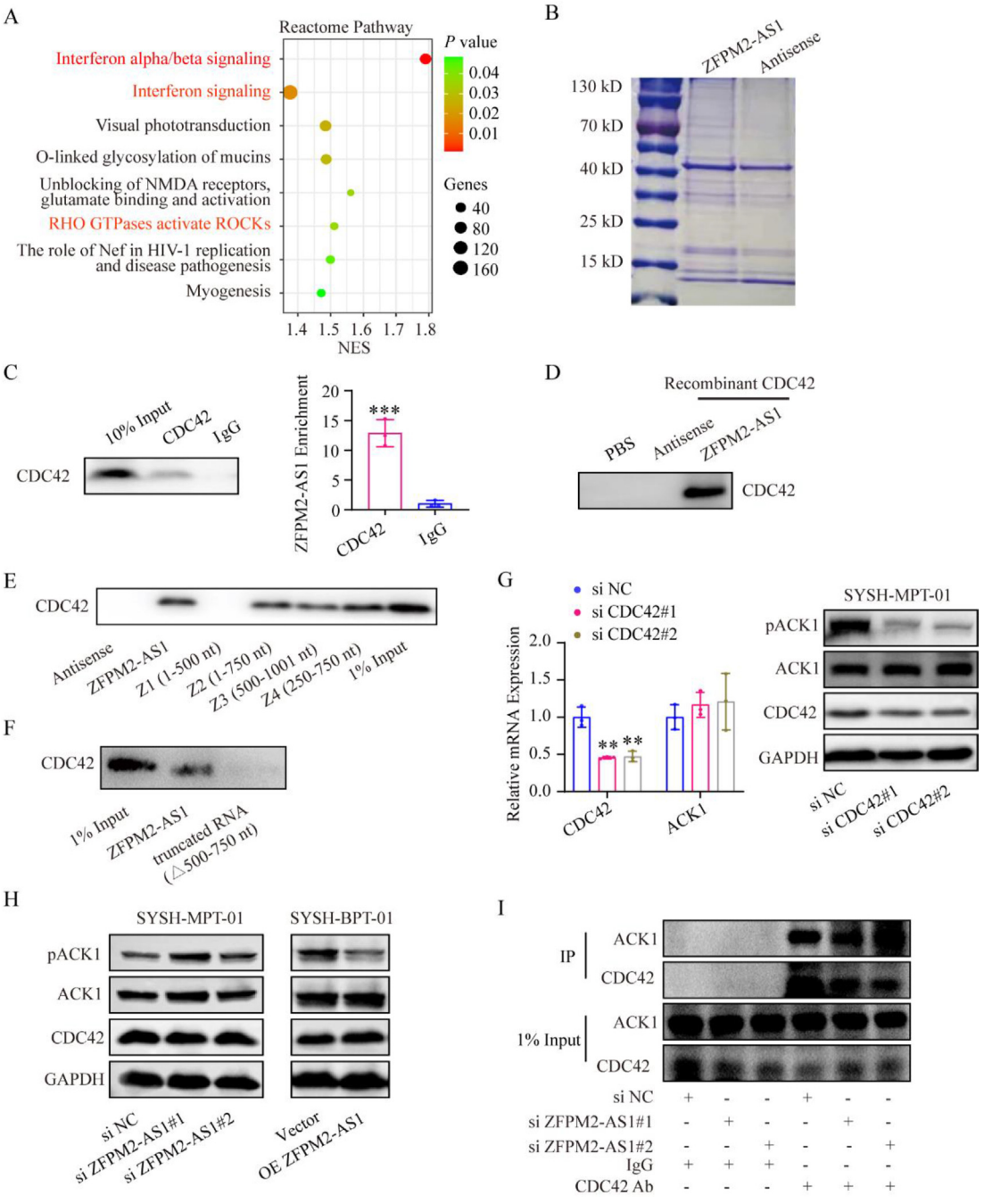

Figure 3 ZFPM2-AS1 competitively binds to CDC42 to disrupt the interaction of ACK1 with CDC42. (A) A bubble map of GSEA pathway enrichment from RNA sequencing reveals significantly up-regulated pathways after ZFPM2-AS1 knockdown. (B) Coomassie brilliant blue staining of RNA pull-down proteins showed multiple differential bands between the ZFPM2-AS1 group and the control (Antisense) group. (C) The binding of ZFPM2-AS1 to CDC42 was verified by RIP assays, the enrichment of CDC42 protein by CDC42 antibody was detected by WB (Left), and the amount of ZFPM2-AS1 in the precipitates was detected by PCR (Right). IgG was the negative control. (D) ZFPM2-AS1 pull-down assays were conducted and CDC42 recombinant protein in the precipitates was measured by WB. PBS and antisense were the blank control and negative control, respectively. (E) RNA pull-down experiments of truncated ZFPM2-AS1, WB was used to detect the amount of CDC42 in the precipitates enriched by the four truncated. Full length of ZFPM2-AS1 and antisense were the positive control and negative control, respectively. (F) RNA pull-down experiments of truncated ZFPM2-AS1 with deletion of the 500−750 nt, WB was used to detect the amount of CDC42 in the precipitates enriched by the truncated RNA. The full length of ZFPM2-AS1 was the positive control. (G) After CDC42 knockdown, the RNA and protein levels of ACK1 in the SYSH-MPT-01 were detected. The knockdown efficiency of CDC42 reached 50%, and the RNA (Left) and total protein levels (Right) of ACK1 remained unchanged, while the phosphorylation level decreased. (H) WB showed the change of ACK1 and CDC42 protein levels in PT cell lines after knockdown (Left) or overexpression (Right) of ZFPM2-AS1. (I) In the co-IP experiment, WB showed that the amount of ACK1 enriched by CDC42 antibody was increased after ZFPM2-AS1 knockdown. Data are shown as mean ± SD, $n = 3$. $^{*}P < 0.05$, $^{**}P < 0.01$, and $^{***}P < 0.001$.

the up-regulated interferon signaling pathway was observed, the results for qRT-PCR revealed that ZFPM2-AS1 knockdown had no significant effect on the expression levels of interferons (IFNA1, IFNB1, and IFNG) (Fig. S3C), indicating that a novel mechanism may activate the interferon signaling pathway and affect the downstream effector molecule. Subsequently, we conducted RNA pull-down assays to identify proteins that interacted with ZFPM2-AS1. Coomassie brilliant blue staining showed significant differences in the proteins pulled down by ZFPM2-AS1 compared to the antisense control group (Fig. 3B). Mass spectrometry analysis for proteins pulled down by ZFPM2-AS1 identified CDC42, with the highest peptide coverage (11%) among the Rho-subfamily. Previous studies have reported that CDC42, which is regulated by the IFNγ-STAT1 pathway, can regulate cell secretion of interferon[16-18]. Interestingly, we observed the interaction between ZFPM2-AS1 and CDC42 by RNA immunoprecipitation (RIP) assays, wherein the CDC42 antibody group enriched a higher concentration of ZFPM2-AS1 compared to the control IgG group (Fig. 3C). In order to ask whether ZFPM2-AS1 directly interacts with CDC42, we conducted RNA pull-down experiments using recombinant CDC42 protein. Supporting this, ZFPM2-AS1 was able to directly bind to CDC42, while no CDC42 was detected in the control antisense group (Fig. 3D). Subsequently, we generated four truncated RNAs of ZFPM2-AS1, namely Z1 (1−500 nt), Z2 (1−750 nt), Z3 (500−1001 nt), and Z4 (250−750 nt) (Fig. S3D), to identify the specific sequences of ZFPM2-AS1 that directly interact with CDC42. The RNA pull-down results suggested that the 500−750 nt region of ZFPM2-AS1 directly bound to CDC42, as CDC42 was enriched in Z2, Z3 and Z4 truncated RNAs (Fig. 3E). Further, we constructed a truncated RNA of ZFPM2-AS1 that deleted the 500−750 nt and conducted RNA pull-down to explore the binding of CDC42 to ZFPM2-AS1. As expected, the results showed that truncated RNA failed to bind to CDC42 (Fig. 3F). These results verify that the 500−750 nt of ZFPM2-AS1 is indispensable for binding with CDC42.

Furthermore, the STRING database implies that CDC42 interacts with a non-receptor tyrosine kinase TNK2, also known as ACK1 (Fig. S3E), leading to the phosphorylation of ACK1 and down-stream target proteins in cells[19,20]. In malignant PT, our result indicated that CDC42 knockdown had no significant effect on ZFPM2-AS1 expression (Fig. S3F) and the RNA and total protein levels of ACK1, but the phosphorylation level of ACK1 was distinctly decreased (Fig. 3G). Surprisingly, when we silenced ZFPM2-AS1 in malignant PT cells, the phosphorylation of ACK1 was significantly increased, while CDC42 expression did not alter (Fig. 3H). Additionally, the results for co-immunoprecipitation assays showed that the level of ACK1 in the CDC42-immunoprecipitated proteins has markedly risen in malignant PT with ZFPM2-AS1 knockdown, suggesting that ZFPM2-AS1 disrupts the orchestration between CDC42 and ACK1 (Fig. 3I). Besides, we performed RIP assays for CDC42 to detect the binding between ZFPM2-AS1 and CDC42 after ACK1 depletion. Our result indicated that ACK1 knockdown led to more ZFPM2-AS1 binding to CDC42, compared to the NC group. This result implies that ACK1 also affects the interplay between ZFPM2-AS1 and CDC42 in PTs (Fig. S3G). Taken together, these findings indicate that the 500−750 nt sequence of ZFPM2-AS1 competitively and directly binds to CDC42, disrupting the binding of CDC42 to ACK1, leading to the inactivation of ACK1 downstream signaling.

3.4. ZFPM2-AS1 upregulates TNFRSF19 expression by inhibiting the activation of ACK1 and STAT1

Furthermore, we investigated the impact of ZFPM2-AS1 on STAT1, a downstream effector molecule of IFN signaling, which has been shown in previous studies to be regulated by ACK1 and involved in the expression of IFN-stimulated genes[21,22]. We examined the RNA and protein levels of STAT1 after knockdown or overexpression of ZFPM2-AS1 in PT cell lines and found that ZFPM2-AS1 did not alter the expression of STAT1, but rather inhibited its phosphorylation (Fig. 4A and B). Besides, we overexpressed truncated ZFPM2-AS1 with deletion of the 500−750 nt in PT cell line and detected the expression and phosphorylation changes of ACK1 and STAT1 by WB. The results showed that truncated ZFPM2-AS1 did not affect the expression and phosphorylation changes of ACK1 and STAT1 (Supporting Information Fig. S4A). To further corroborate that ZFPM2-AS1 inhibits STAT1 activation by suppressing ACK1 phosphorylation in PT, we performed rescue experiments by abrogating ACK1, and observed that ZFPM2-AS1 loss-of-function in PT cell line SYSH-MPT-01 no longer promoted STAT1 phosphorylation (Fig. 4C). These results suggest that ZFPM2-AS1 hinders the phosphorylation of STAT1 by inhibiting ACK1 activation, thereby impacting the interferon pathway.

To figure out the downstream target genes modulated by ZFPM2-AS1 inhibiting STAT1 phosphorylation, we intersected two groups of genes: one group consisted of genes that showed significant correlation with ZFPM2-AS1 expression in the mRNA microarrays (Fig. S4B), and the other group comprised of genes that were differentially expressed after ZFPM2-AS1 knockdown in RNA sequencing (Fig. S4C). Through this intersection, ZFPM2-AS1 expression varies directly as the expression of 966 genes and inversely as the expression of 749 genes (Fig. 4D). Subsequently, in accord with positive correlation with ZFPM2-AS1, the top five genes were chosen and confirmed by qRT-PCR in PT cell line, and eventually the expression of TNFRSF19 was validated as positive correlation with alteration of ZFPM2-AS1 expression (Fig. S4D). Moreover, silencing ZFPM2-AS1 could significantly inhibit the expression of TNFRSF19 (Fig. 4E). TNFRSF19 has been reported to promote malignant progression in tumors such as glioblastoma, melanoma, and nasopharyngeal carcinoma[23-25]. The JASPAR database predicted several binding sites of STAT1 in the promoter region of TNFRSF19 (Fig. 4F). Then, we performed dual luciferase reporter assays to verify the regulation of STAT1 on TNFRSF19 transcription, and the results showed that transcription of TNFRSF19 was significantly intercepted once STAT1 activated by adding IFN-γ, but obviously enhanced by STAT1 loss-of-function (Fig. 4G). To further confirm the role of TNFRSF19 as an effector gene whose expression was modulated by ZFPM2-AS1 inhibiting STAT1 activation, we performed rescue experiments and found that the reduction of STAT1 was able to restore the decline of TNFRSF19 caused by ZFPM2-AS1 knockdown (Fig. 4H). Besides, to establish the causal link between ACK1 activation and TNFRSF19 expression, we performed qRT-PCR and WB to detect the expression of TNFRSF19 in four groups (sh-control, EGF, sh-ZFPM2-AS1, sh-ZFPM2-AS1+si ACK1). Our result indicated that EGF-treated cells increased ACK1 phosphorylation and decreased TNFRSF19 expression. Similarly, ACK1 phosphorylation increased and TNFRSF19 expression decreased in the sh-ZFPM2-AS1 group, while knockdown of

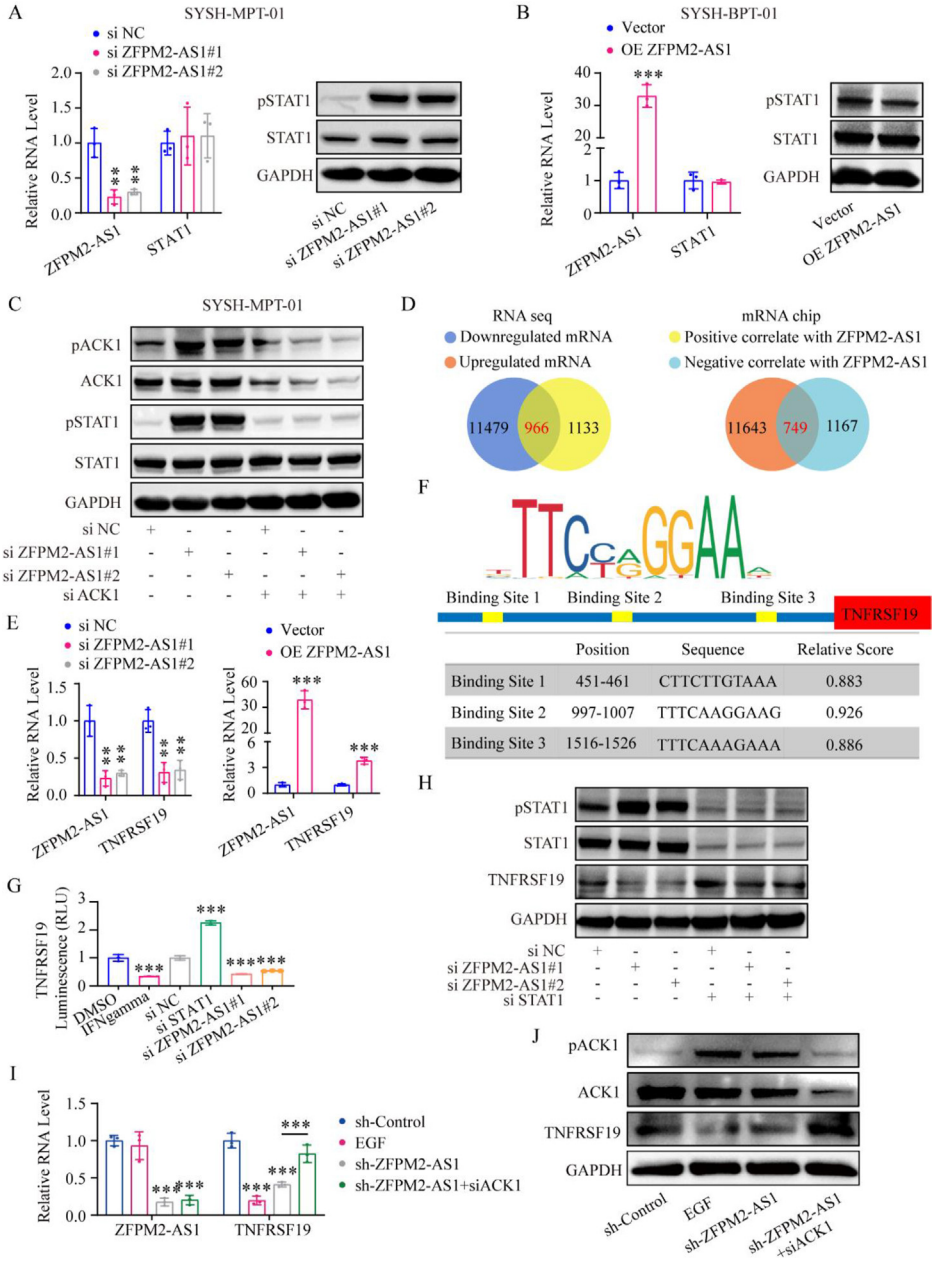

Figure 4 ZFPM2-AS1 upregulates TNFRSF19 expression by inhibiting the activation of ACK1 and STAT1. (A) qRT-PCR showed that the RNA level of STAT1 remained unchanged after ZFPM2-AS1 knockdown (Left), while WB showed that the protein level remained unchanged but the phosphorylation level increased (Right). (B) qRT-PCR showed that the RNA level of STAT1 remained unchanged after ZFPM2-AS1 overexpression (Left), while WB showed that the protein level remained unchanged but the phosphorylation level decreased (Right). (C) Rescue experiments showed that knockdown of ACK1 restored the elevated STAT1 phosphorylation level caused by ZFPM2-AS1 knockdown. (D) 966 genes were obtained by the intersection of the genes that were downregulated after knocking down ZFPM2-AS1 in RNAseq and the genes that were positively correlated with ZFPM2-AS1 in mRNA chip (Left). 749 genes were obtained by the intersection of the genes that were upregulated after knocking down ZFPM2-AS1 in RNAseq and the genes that were negatively correlated with ZFPM2-AS1 in mRNA chip (Right). (E) The expression of TNFRSF19 was remarkably decreased after ZFPM2-AS1 knockdown (Left) and significantly increased after ZFPM2-AS1 overexpression (Right). (F) Prediction of STAT1 binding sites in the TNFRSF19 promoter region by JASPAR database. (G) Dual-luciferase assay showed that knockdown of STAT1 increased the transcriptional activity of TNFRSF19, while interferon stimulation and knockdown of ZFPM2-AS1 decreased the transcriptional activity of TNFRSF19. (H) Rescue experiments showed that knockdown STAT1 restored the decreased TNFRSF19 protein level caused by knockdown ZFPM2-AS1. (I) qRT-PCR showed the expression level of ZFPM2-AS1 and TNFRSF19 in groups of sh-control, EGF, sh-ZFPM2-AS1 and sh-ZFPM2-AS1+si ACK1. (J) WB showed that ACK1 phosphorylation increased and TNFRSF19 expression decreased in the sh-ZFPM2-AS1 group, while knockdown of ZFPM2-AS1, paralleled by ACK1 knockdown, reversed TNFRSF19 expression. Data in (A), (B), (E), (G), (I) are shown as mean ± SD, $n = 3$; $^{*}P < 0.05$, $^{**}P < 0.01$, and $^{***}P < 0.001$.

ZFPM2-AS1, paralleled by ACK1 knockdown, reversed TNFRSF19 expression (Fig. 4I and J). These results indicated that ACK1 activation affects the expression of TNFRSF19. Taken together, these findings provide solid evidence that TNFRSF19 is an effector gene downstream of ZFPM2-AS1-mediated inhibition of STAT1 activation.

To testify the causal link between the TNFRSF19 change and ZFPM2-AS1 intervention, rescue experiments through reconstitution of full-length ZFPM2-AS1 or truncated ZFPM2-AS1 which deleted 500−750 nt in PT cells were performed. In detail, we performed *in vitro* functional assays to detect the cell phenotype. qRT-PCR and WB were utilized to detect the expression level of TNFRSF19 in the cells of four groups (sh-control, sh-ZFPM2-AS1, sh-ZFPM2-AS1+oe-truncated RNA, and sh-ZFPM2-AS1+oe-full length RNA). The qRT-PCR and WB showed that overexpressed full-length or truncated ZFPM2-AS1 could both rescue the ZFPM2-AS1 level, but reconstitution of truncated ZFPM2-AS1 failed to rescue the expression of TNFRSF19 (Fig. S4E and S4F). The functional assays indicated that reconstitution of full-length ZFPM2-AS1 could rescue the cell proliferation, migration, and invasion abilities which were inhibited by knocking down ZFPM2-AS1, while reconstitution of truncated ZFPM2-AS1 could not rescue them (Fig. S4G−S4I).

3.5. *Nanoparticle Meo-PEG-b-PDPA is an effective carrier to deliver ZFPM2-AS1 siRNA*

Recent studies have revealed that nucleic acid drugs, such as antisense oligonucleotides and small interfering RNA (siRNA), can be effectively delivered into tumor cells through the use of nanoparticles (NPs)[15,26]. NPs can markedly prolong the half-life of nucleic acid *in vivo*, and ameliorate their ability to penetrate tumor cell membranes, which facilitates accurate and efficient treatment of malignant tumors. To verify the effect of ZFPM2-AS1 on PT progression *in vivo*, we utilized NPs with endosomal pH-responsiveness to encapsulate ZFPM2-AS1-targeting siRNA. The NPs used in our study were composed of methoxyl-poly (ethylene glycol)-*b*-poly (2-(diisopropylamino) ethyl methacrylate) (Meo-PEG-*b*-PDPA) polymer, with a pK_a of approximately 6.30 (Fig. 5A) and had a size of about 69 nm[15]. When the environmental pH was higher than the pK_a, the NPs tightly encapsulated siRNA in its interior, however, upon endocytosis into the endosomes, the NPs responded to the acidic pH of the endosomes (pH 6.0−6.5), leading to dispersion and rapid release of the encapsulated siRNA, thereby enhancing the gene silencing effect of siRNA[27] (Fig. 5B). Initially, we encapsulated NC or ZFPM2-AS1 siRNA in Meo-PEG-*b*-PDPA, and found that the size and zeta potential of NPs encapsulating NC siRNA (NPs-NC siRNA) and ZFPM2-AS1 siRNA (NPs-ZFPM2-AS1 siRNA) had no significantly different (Fig. 5C, Supporting Information Fig. S5A). Subsequently, we evaluated the knockdown efficiency of NPs-ZFPM2-AS1 siRNA using PT cell lines *in vitro* and found that the knockdown efficiency could reach 70% (Fig. S5B).

To assess the *in vivo* delivery capability of NPs, we intravenously injected Cy5-labeled naked siRNA and NPs siRNA into BALB/c mice. We conducted a pharmacokinetic experiment by monitoring the fluorescence signal in the blood of the mice. The results revealed that naked siRNA was rapidly degraded, with less than 1% remaining after 30 min, whereas NPs siRNA still had around 40% residual amount 2 h after injection (Fig. 5D). Furthermore, to assess the distribution of siRNA, we injected Cy5-labeled naked siRNA and NPs siRNA into PDX mice of PT, collected the PTs and viscera of the mice 24 h later. The results demonstrated that the signal of Cy5 in tumors of NPs group was significantly higher than that of the control group (Fig. 5E). Besides, to detect the knockdown efficiency of NPs-ZFPM2-AS1 siRNA *in vivo*, we injected NPs-NC siRNA and NPs-ZFPM2-AS1 siRNA into PDX mice of PT, extracted tissue RNA of PTs from PDX mice and conducted qRT-PCR, which revealed a significant reduction in the expression of ZFPM2-AS1 in the NPs-ZFPM2-AS1 siRNA group compared to the control group. Similar results were obtained through ISH staining (Fig. 5F). Collectively, these findings from our experiments demonstrate that the use of NPs can significantly improve the enrichment of siRNA at the site of PT, which facilitates siRNA to effectively exert its gene silencing effect *in vivo*.

To assess the systemic toxicity of NPs-siRNA, healthy BALB/c mice were injected with PBS, NPs-NC siRNA, and NPs-ZFPM2-AS1 siRNA, and were euthanized 24 h later. Blood was collected to measure the levels of liver enzymes, urea, and creatinine to monitor the liver and kidney function. Surprisingly, there was no obvious distinction in the levels of liver enzymes, urea, and creatinine in plasma between the NPs-siRNA groups and the PBS group (Fig. S5C), confirming the safety of NPs-siRNA *in vivo*. In addition, HE staining for the heart, liver, spleen, lung, and kidney organs of mice showed that the tissue structure of these vital organs was not subjected to significant alteration caused by NPs-siRNA injection (Fig. S5D). Collectively, these *in vivo* assays prove that NPs-siRNA has no obvious toxicity to organs.

3.6. *ZFPM2-AS1 knockdown effectively inhibited the growth and metastasis of malignant PT in mice*

In the *in vivo* study, PDX mice were divided into three groups: PBS, NPs-NC siRNA, and NPs-ZFPM2-AS1 siRNA. After three consecutive intravenous injections of siRNA, tumor size was measured periodically to observe the effect of ZFPM2-AS1 siRNA on PTs (Fig. 6A). The tumor volume growth curve illustrated that the PTs in the NPs-ZFPM2-AS1 siRNA group grew significantly slower, in contrast to the NPs-NC siRNA group and PBS group (Fig. 6B). Fifteen days after NPs-siRNA injection, the tumor size of the NPs-ZFPM2-AS1 siRNA group was markedly smaller than that of the NPs-NC siRNA and PBS groups was further corroborated through collecting PTs of PDX mice (Fig. 6C). These results revealed that knocking down ZFPM2-AS1 could significantly impede PT growth *in vivo*. The expression of STAT1, ACK1, and TNFRSF19 was further measured by qRT-PCR according to RNA extracted from PTs. Coinciding with our expect, knockdown of ZFPM2-AS1 *in vivo* had no influence on mRNA levels of STAT1 and ACK1 but significantly reduced mRNA level of TNFRSF19 (Fig. 6D). IHC further elucidated that ZFPM2-AS1 reduction distinctly promoted phosphorylation of STAT1 and ACK1 and decreased TNFRSF19 expression in PDX tumors (Fig. 6E).

Besides, to explore the metastatic potential of PT cells *in vivo*, we divided NOD-SCID female mice into two groups (7 mice per group): sh-control and sh-ZFPM2-AS1. The corresponding cells

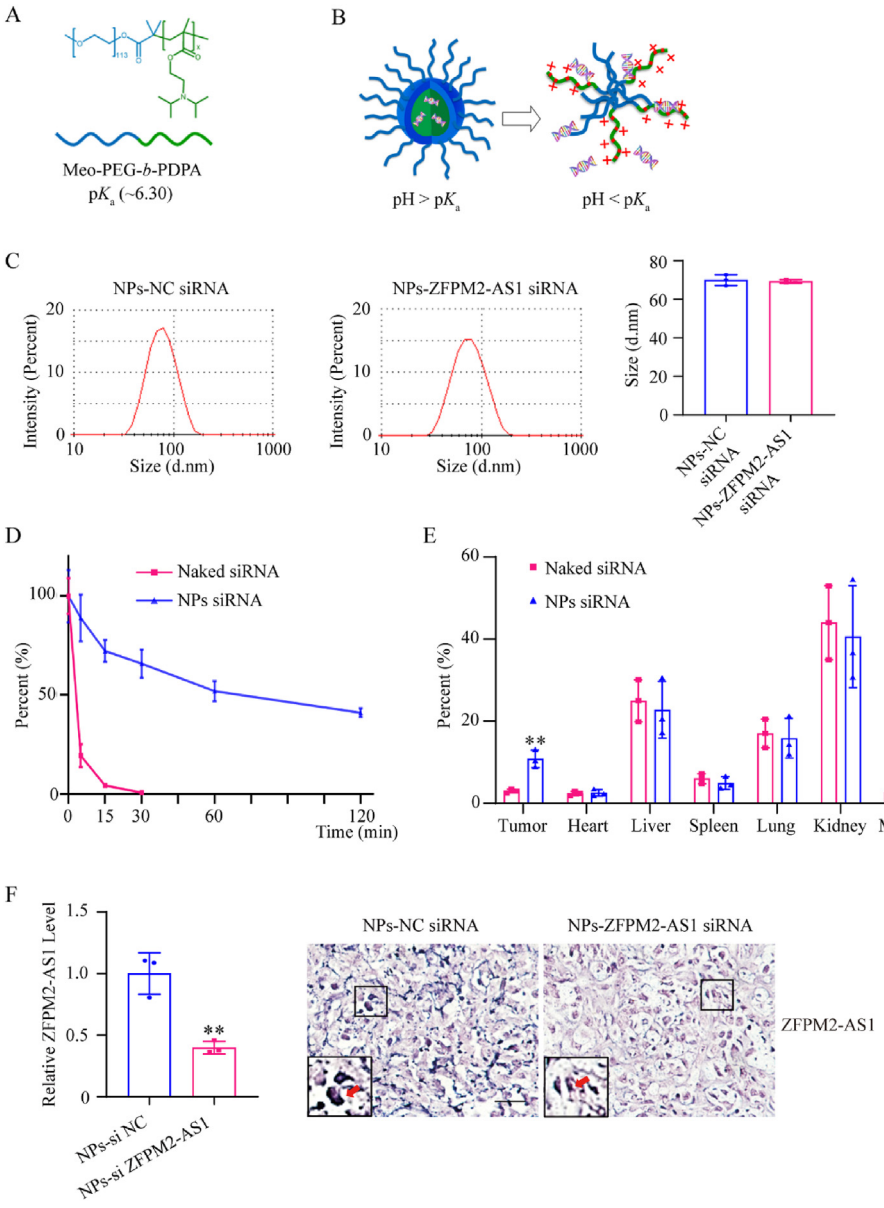

Figure 5 Nanoparticle Meo-PEG-*b*-PDPA is an effective carrier to deliver ZFPM2-AS1 siRNA. (A) Molecular structure diagram of nanomaterial methoxyl-poly(ethylene glycol)-*b*-poly(2-(diisopropylamino) ethyl methacrylate) (Meo-PEG-*b*-PDPA). (B) A schematic diagram shows that the nanoparticles with endosomal pH-responsiveness gather into a sphere when the ambient pH is greater than pK_a, and depolymerize to release the encapsulated matter when the ambient pH is less than pK_a. (C) The size of the nanoparticles containing NC siRNA and ZFPM2-AS1 siRNA was similar. (D) The pharmacokinetic experiment showed that NPs-Cy5-siRNA had a longer half-life in mice than naked Cy5-siRNA. (E) The biodistribution of the Cy5-siRNA in the tumors and major organs of the PDX mice was detected. Bar chart showed the concentration of NPs-Cy5-siRNA in PDX mice tumors was significantly higher than that of naked Cy5-siRNA. (F) qRT-PCR (Left) and ISH (Right) showed that the expression of ZFPM2-AS1 (blue purple) in PDX tumor tissue in NPs-ZFPM2-AS1 siRNA group was lower than that in NPs-NC siRNA group. Scale bar: 50 μm, red arrows indicate ZFPM2-AS1 expression in cells. Data in (E), (F) are shown as mean ± SD, $n = 3$. $^*P < 0.05$, $^{**}P < 0.01$, and $^{***}P < 0.001$.

(10^7 cells per mouse) were injected into the tail vein of the mice, and the lungs were removed 1 month later to observe the metastasis. Focal lesions were observed in the lungs of the mice (Fig. S5E), then paraffin embedding and HE staining were used to observe the tissue structure and these lesions were eventually identified as lung metastasis (Fig. 6F). We found that 6 of 7 mice in the sh-control group had several lung metastases, while in the sh-ZFPM2-AS1 group, only 1 mouse had a metastasis (Fig. 6G

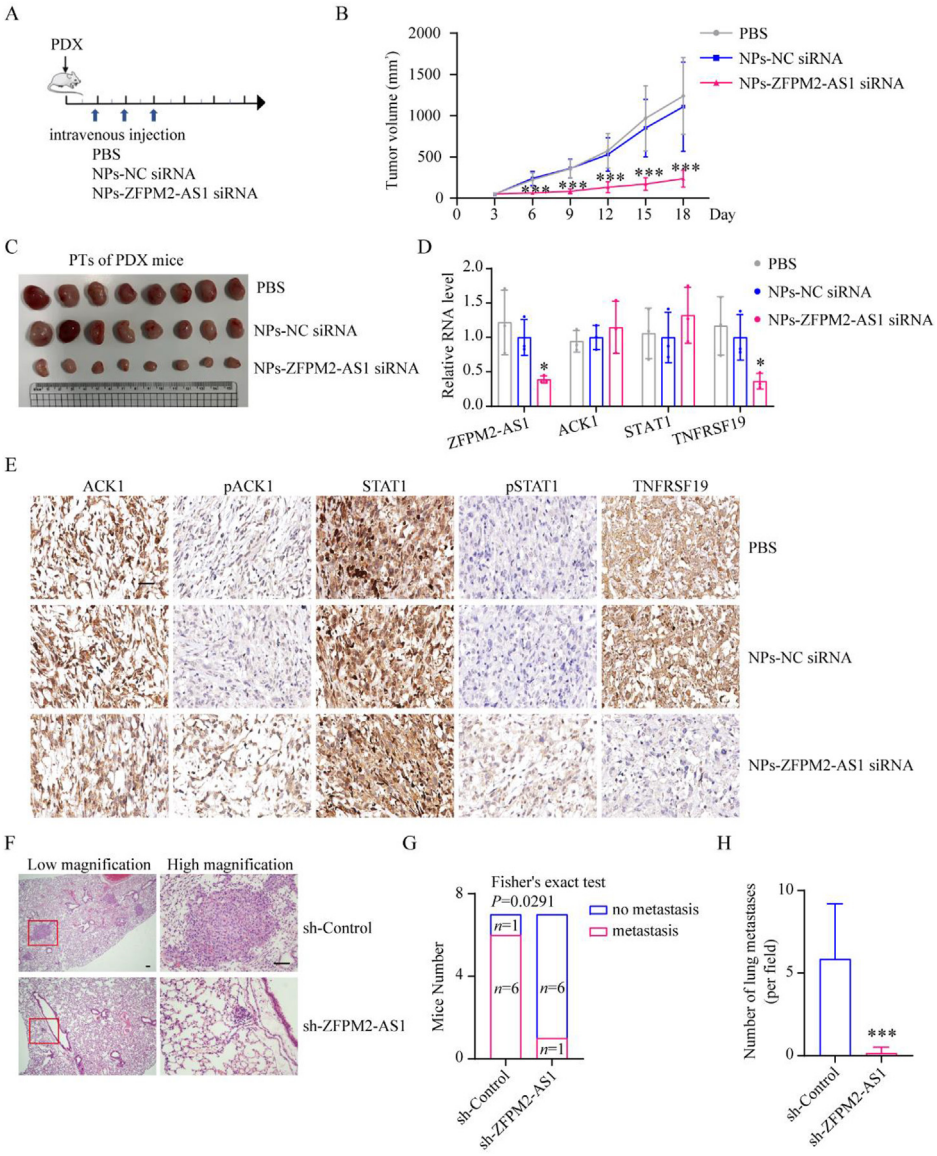

Figure 6 ZFPM2-AS1 knockdown effectively inhibited the growth and metastasis of malignant PT in mice. (A). Schematic illustration of detection of tumor growth inhibition by ZFPM2-AS1 siRNA *in vivo*. PDX mice with PT were given three consecutive intravenous injections of NPs-siRNA (1 nmol/mice), followed by tumor size measurements every three days. (B) The tumor growth curve showed that NPs-ZFPM2-AS1 siRNA significantly inhibited PT growth in PDX mice. Data was shown as mean ± SD, $n = 8$; $^{*}P < 0.05$, $^{**}P < 0.01$, and $^{***}P < 0.001$. (C) Tumor images of PDX mice in PBS group, NPs-NC siRNA group, and NPs-ZFPM2-AS1 siRNA group 18 days after injection. (D) qRT-PCR showed that NPs-ZFPM2-AS1 siRNA had no significant effect on the RNA level of ACK1 and STAT1 in PT of PDX mice compared with NPs-NC siRNA, but the expression of TNFRSF19 was significantly decreased. Data was shown as mean ± SD, $n = 3$. $^{*}P < 0.05$, $^{**}P < 0.01$, and $^{***}P < 0.001$. (E) IHC showed that NPs-ZFPM2-AS1 siRNA had no significant effect on the protein levels of ACK1 and STAT1 in PT of PDX mice compared with NPs-NC siRNA, but the phosphorylation levels of ACK1 and STAT1 were significantly increased, and the protein levels of TNFRSF19 were greatly decreased. Scale bar: 50 μm. (F) Representative HE staining showed the histological features of lung metastases in the sh-control group and sh-ZFPM2-AS1 group. The red box showed the lung metastases. Scale bar: 50 μm. (G) Bar chart showed that 6 of 7 mice in the sh-control group had lung metastases, while in the sh-ZFPM2-AS1 group, only one mouse had lung metastases. Fisher's exact test indicated a significant difference between the two groups. (H) The number of lung metastases under low magnification in the sh-control group was significantly higher than that in the sh-ZFPM2-AS1 group. Data are shown as mean ± SD, $n = 7$; $^{*}P < 0.05$, $^{**}P < 0.01$, and $^{***}P < 0.001$.

and H), and the lung metastasis in the sh-ZFPM2-AS1 group was obviously smaller than those in the sh-control group (Fig. 6F), indicating that ZFPM2-AS1 depletion significantly reduced the metastatic potential of PT cells in mice.

4. Discussion

Up to now, clinical diagnosis and grading of breast PT exclusively rely on morphological indicators, which lack clear cutoff values

and are subjective, further resulting in limitations in predicting patient prognosis. Besides, the lack of effective treatment for malignant PT causes a high mortality rate.

In this study, we identified a lncRNA defined as ZFPM2-AS1 in PT for the first time and found that it was closely related to high tumor grade and poor patient outcomes. In our previous studies, we proposed a prediction model based on the width of surgical margin, mitoses, and tumor border, and used a nomogram to predict PT patient prognosis[28]. However, this model still lacks objective indicators. Here, we found that the expression of ZFPM2-AS1 in frozen PT tissues was significantly positively correlated with malignant pathological features of PT, and further using ISH of paraffin sections and survival analysis revealed that patients with high expression of ZFPM2-AS1 had a significantly worse prognosis. Therefore, the expression level of ZFPM2-AS1 can be considered as a potential addition to the prognostic model to improve its feasibility and accuracy in future.

ZFPM2-AS1 was reported as a tumor-promoting lncRNA in lung cancer, gastric cancer, colorectal cancer, and liver hepatocellular carcinoma, which is consistent with our results for the role of ZFPM2-AS1 in PT. For instance, Min Xue et al. illustrate that ZFPM2-AS1 competitively binds with miR-18b-5p and promotes the expression of VMA21, leading to the proliferation of lung adenocarcinoma cells[29]. Kong et al.[30] prove that ZFPM2-AS1 binds to and protects the degradation of macrophage migration inhibitory factor (MIF), inhibiting p53 protein activation and nuclear translocation, and thereby promoting proliferation and inhibiting apoptosis of gastric cancer cells. He et al.[31] show that ZFPM2-AS1 competitively binds to miR-139 and promotes the expression of GDF10 to enhance cell invasion in liver hepatocellular carcinoma. These studies collectively indicate that ZFPM2-AS1 is significantly associated with the malignant phenotype of tumors and has the potential to be used as a diagnostic marker and therapeutic target for malignant tumors.

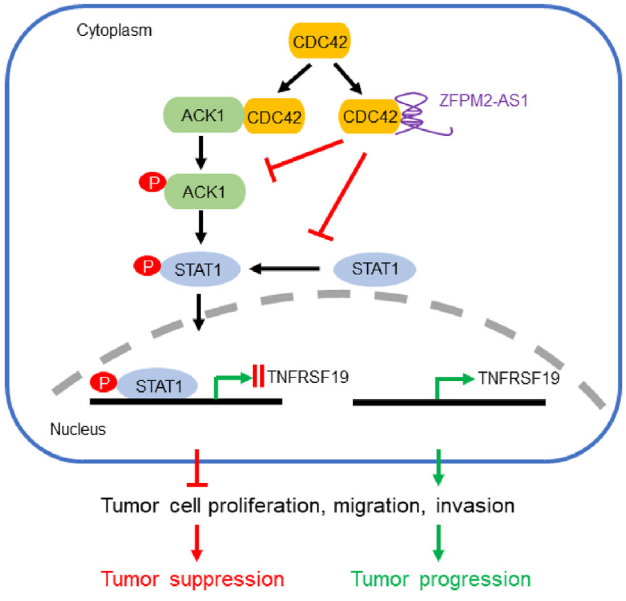

Figure 7 Schematic showing the mechanism by which ZFPM2-AS1 promotes malignant progression in PT.

While previous studies have suggested an association between ZFPM2-AS1 expression and poor clinical outcomes, they have not explored ZFPM2-AS1 as a therapeutic target for malignant tumors. In this study, we used NPs to deliver ZFPM2-AS1 siRNA into PDX mice of PT and successfully knocked down ZFPM2-AS1 expression, confirming the inhibitory effect of ZFPM2-AS1 siRNA on PT growth *in vivo*. Additionally, toxicity tests in healthy mice showed the safety of intravenous administration of NPs-ZFPM2-AS1 siRNA. As PT is not sensitive to chemotherapy and lacks effective therapeutic means to control the recurrence and metastasis[4,32], our consolidated data lays a solid foundation to underpin the potential application of ZFPM2-AS1 siRNA as a specific molecular therapy for malignant PT with a poor prognosis in the future.

Besides, our *in vitro* experiments revealed that ZFPM2-AS1 can competitively bound to CDC42, resulting in the inhibition of the ACK1 activation, which in turn reduces STAT1 activation, leading to the release of transcriptional inhibition on the tumor-promoting molecule TNFRSF19 and thereby promoting the proliferation, migration, and invasion of breast PT (Fig. 7). CDC42, a small Rho GTPase, is highly expressed or overactivated in various malignant tumors and closely related to tumor occurrence, invasion, and metastasis[33,34], including both an activation state of GTP binding and a deactivation state of GDP binding, and ACK1 specifically binds to the activated form of CDC42[35,36]. In our study, we found that perturbation of ZFPM2-AS1 expression did not alter CDC42 expression, but whether the combination of ZFPM2-AS1 and CDC42 affects the activation state of CDC42 remains unclear. Further exploration of the role of CDC42 activation in the growth and metastasis of PT is warranted in future studies. In addition, our RNA-seq analysis showed that interferon pathway-associated genes were significantly up-regulated after ZFPM2-AS1 knockdown. The interferon signaling pathway is a major component of innate immunity which plays an important role in host resistance to pathogens. Therefore, it would be worthwhile to further investigate whether ZFPM2-AS1 participates in anti-tumor immunity in the tumor microenvironment through inhibiting the interferon signaling pathway.

5. Conclusions

In conclusion, our findings expound for the first time on the role of ZFPM2-AS1 in PT and highlight the potential of ZFPM2-AS1 siRNA as a therapeutic target for malignant PT, as supported by our *in vitro* and *in vivo* experiments.

Acknowledgments

We thank all members of the breast cancer center for helpful suggestions. We also appreciate the assistance from the Disease Registry Department of Sun Yat-sen Memorial Hospital, Sun Yat-sen University. This work was supported by the National Natural Science Foundation of China (82173054, 82222029, 82203085), the Guangdong Basic and Applied Basic Research Foundation (2022B1515020048, 2022B1515020101, China), Guangzhou Science, Technology and Innovation Commission (20210 2010148, China).

Author contributions

Shishi He: Data curation; formal analysis; validation; visualization; methodology; writing − original draft; writing − review and editing. Guowei Huang: Conceptualization; data curation; formal analysis; validation; methodology; writing − review and editing. Rong Lei: Data curation; formal analysis; validation; visualization; methodology; writing − original draft; writing − review and editing. Rurong Jia: Data curation; formal analysis; validation. Zhanghai He: Data curation; formal analysis; validation. Jiewen Chen: Data curation; formal analysis; validation; visualization; methodology. Hongyan Huang: Data curation; formal analysis; validation; methodology. Zixian Huang: Formal analysis; validation; visualization; methodology. Ailifeire Yilihamu: Formal analysis; investigation; methodology. Xun Li: Software; formal analysis. Zilin Zhuang: Formal analysis; investigation. Mengjia Han: Formal analysis; investigation. Xueman Chen: Conceptualization; resources; supervision; formal analysis; writing − original draft; writing − review and editing. Di Huang: Conceptualization; resources; supervision; formal analysis; writing − original draft; project administration; writing − review and editing. Yan Nie: Conceptualization; resources; supervision; funding acquisition; formal analysis; writing − original draft; project administration; writing − review and editing.

Conflicts of interest

The authors declare that they have no conflict of interest.

Appendix A. Supporting information

Supporting information to this article can be found online at https://doi.org/10.1016/j.apsb.2024.04.023.

References

1. Rayzah M. Phyllodes tumors of the breast: a literature review. *Cureus* 2020;**12**:e10288.
2. Lebeau A. Updated WHO classification of tumors of the breast. *Pathologe* 2021;**42**(Suppl 2):155−9.
3. Zhou ZR, Wang CC, Sun XJ, Yang ZZ, Chen XX, Shao ZM, et al. Prognostic factors in breast phyllodes tumors: a nomogram based on a retrospective cohort study of 404 patients. *Cancer Med* 2018;**7**:1030−42.
4. Ramakant P, Chakravarthy S, Cherian JA, Abraham DT, Paul MJ. Challenges in management of phyllodes tumors of the breast: a retrospective analysis of 150 patients. *Indian J Cancer* 2013;**50**:345−8.
5. Kim S, Kim JY, Kim DH, Jung WH, Koo JS. Analysis of phyllodes tumor recurrence according to the histologic grade. *Breast Cancer Res Treat* 2013;**141**:353−63.
6. Wang ZC, Buraimoh A, Iglehart JD, Richardson AL. Genome-wide analysis for loss of heterozygosity in primary and recurrent phyllodes tumor and fibroadenoma of breast using single nucleotide polymorphism arrays. *Breast Cancer Res Treat* 2006;**97**:301−9.
7. Chao X, Chen K, Zeng J, Bi Z, Guo M, Chen Y, et al. Adjuvant radiotherapy and chemotherapy for patients with breast phyllodes tumors: a systematic review and meta-analysis. *BMC Cancer* 2019;**19**:372.
8. Cserni G. Histological type and typing of breast carcinomas and the WHO classification changes over time. *Pathologica* 2020;**112**:25−41.
9. Ponting CP, Oliver PL, Reik W. Evolution and functions of long noncoding RNAs. *Cell* 2009;**136**:629−41.
10. Schmitt AM, Chang HY. Long noncoding RNAs in cancer pathways. *Cancer Cell* 2016;**29**:452−63.
11. Gutschner T, Hammerle M, Eissmann M, Hsu J, Kim Y, Hung G, et al. The noncoding RNA MALAT1 is a critical regulator of the metastasis phenotype of lung cancer cells. *Cancer Res* 2013;**73**:1180−9.
12. Kogo R, Shimamura T, Mimori K, Kawahara K, Imoto S, Sudo T, et al. Long noncoding RNA HOTAIR regulates polycomb-dependent chromatin modification and is associated with poor prognosis in colorectal cancers. *Cancer Res* 2011;**71**:6320−6.
13. Nie Y, Huang H, Guo M, Chen J, Wu W, Li W, et al. Breast phyllodes tumors recruit and repolarize tumor-associated macrophages *via* secreting CCL5 to promote malignant progression, which can be inhibited by CCR5 inhibition therapy. *Clin Cancer Res* 2019;**25**:3873−86.
14. He S, Xiao X, Lei R, Chen J, Huang H, Yilihamu A, et al. Establishment of breast phyllodes tumor cell lines preserving the features of phyllodes tumors. *BIO Integration* 2023;**4**:7−17.
15. Xu X, Wu J, Liu Y, Yu M, Zhao L, Zhu X, et al. Ultra-pH-responsive and tumor-penetrating nanoplatform for targeted siRNA delivery with robust anti-cancer efficacy. *Angew Chem Int Ed Engl* 2016;**55**:7091−4.
16. Pulecio J, Petrovic J, Prete F, Chiaruttini G, Lennon-Dumenil AM, Desdouets C, et al. Cdc42-mediated MTOC polarization in dendritic cells controls targeted delivery of cytokines at the immune synapse. *J Exp Med* 2010;**207**:2719−32.
17. Chemin K, Bohineust A, Dogniaux S, Tourret M, Guegan S, Miro F, et al. Cytokine secretion by $CD4^+$ T cells at the immunological synapse requires Cdc42-dependent local actin remodeling but not microtubule organizing center polarity. *J Immunol* 2012;**189**:2159−68.
18. Hu Y, Hu X, Boumsell L, Ivashkiv LB. IFN-gamma and STAT1 arrest monocyte migration and modulate RAC/CDC42 pathways. *J Immunol* 2008;**180**:8057−65.
19. Kato-Stankiewicz J, Ueda S, Kataoka T, Kaziro Y, Satoh T. Epidermal growth factor stimulation of the ACK1/Dbl pathway in a Cdc42 and Grb2-dependent manner. *Biochem Biophys Res Commun* 2001;**284**:470−7.
20. Mahajan K, Mahajan NP. Shepherding AKT and androgen receptor by Ack1 tyrosine kinase. *J Cell Physiol* 2010;**224**:327−33.
21. Fujimoto Y, Ochi H, Maekawa T, Abe H, Hayes CN, Kumada H, et al. A single nucleotide polymorphism in activated Cdc42 associated tyrosine kinase 1 influences the interferon therapy in hepatitis C patients. *J Hepatol* 2011;**54**:629−39.
22. Mahendrarajah N, Borisova ME, Reichardt S, Godmann M, Sellmer A, Mahboobi S, et al. HSP90 is necessary for the ACK1-dependent phosphorylation of STAT1 and STAT3. *Cell Signal* 2017;**39**:9−17.
23. Ding Z, Kloss JM, Tuncali S, Tran NL, Loftus JC. TROY signals through JAK1−STAT3 to promote glioblastoma cell migration and resistance. *Neoplasia* 2020;**22**:352−64.
24. Spanjaard RA, Whren KM, Graves C, Bhawan J. Tumor necrosis factor receptor superfamily member TROY is a novel melanoma biomarker and potential therapeutic target. *Int J Cancer* 2007;**120**:1304−10.
25. Deng C, Lin YX, Qi XK, He GP, Zhang Y, Zhang HJ, et al. TNFRSF19 inhibits TGFbeta signaling through interaction with TGFbeta receptor type I to promote tumorigenesis. *Cancer Res* 2018;**78**:3469−83.
26. Shahbazi R, Ozpolat B, Ulubayram K. Oligonucleotide-based theranostic nanoparticles in cancer therapy. *Nanomedicine* 2016;**11**:1287−308.
27. Deirram N, Zhang C, Kermaniyan SS, Johnston APR, Such GK. pH-responsive polymer nanoparticles for drug delivery. *Macromol Rapid Commun* 2019;**40**:e1800917.
28. Chao X, Jin X, Tan C, Sun P, Cui J, Hu H, et al. Re-excision or "wait and watch"-a prediction model in breast phyllodes tumors after surgery. *Ann Transl Med* 2020;**8**:371.
29. Xue M, Tao W, Yu S, Yan Z, Peng Q, Jiang F, et al. LncRNA ZFPM2-AS1 promotes proliferation *via* miR-18b-5p/VMA21 axis in lung adenocarcinoma. *J Cell Biochem* 2020;**121**:313−21.

30. Kong F, Deng X, Kong X, Du Y, Li L, Zhu H, et al. ZFPM2-AS1, a novel lncRNA, attenuates the p53 pathway and promotes gastric carcinogenesis by stabilizing MIF. *Oncogene* 2018;**37**:5982−96.
31. He H, Wang Y, Ye P, Yi D, Cheng Y, Tang H, et al. Long noncoding RNA ZFPM2-AS1 acts as a miRNA sponge and promotes cell invasion through regulation of miR-139/GDF10 in hepatocellular carcinoma. *J Exp Clin Cancer Res* 2020;**39**:159.
32. Parkes A, Wang WL, Patel S, Leung CH, Lin H, Conley AP, et al. Outcomes of systemic therapy in metastatic phyllodes tumor of the breast. *Breast Cancer Res Treat* 2021;**186**:871−82.
33. Murphy NP, Mott HR, Owen D. Progress in the therapeutic inhibition of Cdc42 signalling. *Biochem Soc Trans* 2021;**49**:1443−56.
34. Murphy NP, Binti Ahmad Mokhtar AM, Mott HR, Owen D. Molecular subversion of Cdc42 signalling in cancer. *Biochem Soc Trans* 2021;**49**:1425−42.
35. Hodge RG, Ridley AJ. Regulating Rho GTPases and their regulators. *Nat Rev Mol Cell Biol* 2016;**17**:496−510.
36. Manser E, Leung T, Salihuddin H, Tan L, Lim L. A non-receptor tyrosine kinase that inhibits the GTPase activity of p21cdc42. *Nature* 1993;**363**:364−7.